JCTC Journal of Chemical Theory and Computation
Article
pubs.acs.org/JCTC

Efficient Self-Consistent Implementation of Local Hybrid Functionals

Hilke Bahmann* and Martin Kaupp

Department of Chemistry, Technische Universität Berlin, Theoretische Chemie - Quantenchemie, Sekr. C7, Straße des 17. Juni 135, 10623 Berlin, Germany

ABSTRACT: Local hybrid density functionals, with position-dependent exact-exchange admixture, are an important extension to the popular global hybrid functionals, promising improved accuracy for many properties. An efficient implementation is crucial to make local hybrids available for widespread application. The resolution-of-the-identity approach used in previous implementations to compute nonstandard two-electron integrals has been found to require large uncontracted basis sets, rendering the cost of local hybrid calculations impractical for large-scale systems. On the basis of recently promoted seminumerical implementations of exact exchange in global hybrid functionals, we present an efficient, self-consistent implementation of local hybrid functionals within the generalized Kohn−Sham scheme. The final cost of a local hybrid calculation is equal to that of a meta-GGA global hybrid using the seminumerical algorithm. Since seminumerical schemes exhibit superior scaling with respect to system and basis set size over analytical exact exchange, and this advantage is not affected by a position-dependent admixture of exact exchange, local hybrid calculations for large systems are now possible.

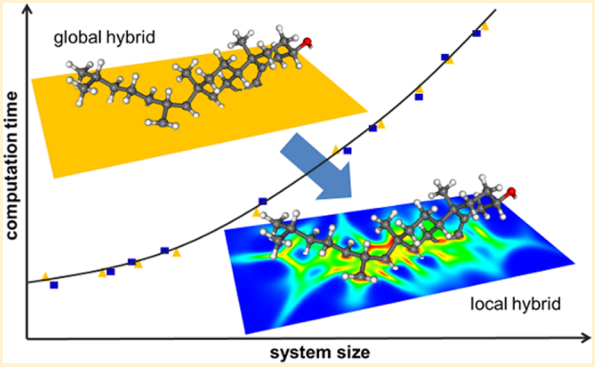

INTRODUCTION

In global hybrid exchange-correlation (XC) functionals of density functional theory (DFT), a portion of the DFT exchange is replaced by the exact-exchange energy from the Hartree−Fock approximation

$$E_{XC}^{gh} = a_0 E_X^{exact} + (1 - a_0) E_X^{DFT} + E_C \quad (1)$$

The mixing coefficient and other parameters can be obtained from a fit to experimental data, from physical constraints, or from a combination of both.[1−4] In any case, the success of hybrid functionals reflects a compromise between the cancellation of one-electron self-interaction by exact exchange and the inclusion of static correlation mimicked by the semilocal density-functional exchange. Aiming for more flexibility, two major approaches to refine such a global hybrid scheme in DFT have been promoted: range separation and position-dependent mixing in real space.

In range-separated hybrid functionals, the exact exchange is screened as a function of the interelectronic distance (e.g., CAM-B3LYP, HSE, and many others).[5,6] While exact exchange in the long-range part leads, e.g., to improved performance for charge transfer or Rydberg excitations in time-dependent DFT (TDDFT) schemes, restricting the exact exchange to short range has been shown to be very useful in extended systems.

Mixing of the exact-exchange and semilocal (sl) exchange energy densities through a real-space-dependent local mixing function (LMF) $a(\mathbf{r})$, on the other hand, leads to the local hybrid (Lh) scheme[7]

$$E_{XC}^{Lh} = \int a(\mathbf{r})\, \epsilon_X^{ex}(\mathbf{r})\, d\mathbf{r} + \int (1 - a(\mathbf{r}))\epsilon_X^{sl}(\mathbf{r})\, d\mathbf{r} + E_C^{sl} \quad (2)$$

To ensure broad applicability of Lhs to systems of chemical interest, three issues need to be considered: (i) the LMF, (ii) the compatibility of the semilocal exchange-energy density with the exact-exchange one (also called the gauge problem), and (iii) an efficient implementation. Several LMFs that fulfill exact constraints and that may contain empirical parameters and possible routes to nonempirical functions have been proposed[7−12] over the last 10 years. Quite accurate results can be obtained for atomization energies, barrier heights, ionization potentials, and other properties, revealing the high potential of this family of functionals. Also, the gauge problem, which is based on the ambiguity of energy densities, and explicit solutions to it by construction of gauge functions have been discussed. Work in this field is an ongoing process and closely intertwined with the derivation of refined LMFs.[13,14] Overall, the Lh scheme promises enhanced accuracy compared to that of global hybrids in many areas of application. Further extensions may involve different combinations between range separation and Lh ideas.[15,16]

A few algorithms for the self-consistent implementation of local hybrids have been reported. Because the additional, nonstandard integrals appearing in the associated potential cannot be solved analytically, all of these implementations so far have relied on a resolution of the identity (RI), expanding the

Received: December 16, 2014
Published: March 11, 2015

DOI: 10.1021/ct501137x
J. Chem. Theory Comput. 2015, 11, 1540−1548

exact-exchange potential in the atomic-orbital basis set.[17] One generalized Kohn−Sham (GKS) implementation has also has been extended to functionals with local range separation.[18] Others include the additional step of localizing the potential within the KLI and/or localized Hartree−Fock approximations to the optimized effective potential.[9,19] So far, neither the efficiency nor the accuracy of such an implementation has been addressed. However, it has already been noted that, within the RI approximation, large uncontracted basis sets are required, rendering this scheme impractical for general applications to large systems.[17,18,20] An efficient and accurate implementation of local hybrid functionals is mandatory to make them available for real applications.

As an alternative to the RI-based approaches, numerical treatments of the nonstandard exact-exchange-based integrals should be considered. Seminumerical implementations of exact exchange go back to Friesner's pseudospectral approaches.[21] Simplified seminumerical schemes for treating exact exchange in global hybrid functionals using a so-called chain-of-spheres algorithm (COSX)[22] have been promoted. For large systems, the seminumerical approaches exhibit linear scaling with system size and overall better scaling with respect to the number of basis functions as compared to that with analytical implementations of exact exchange. A similar implementation (senex) has been realized in the TURBOMOLE[23] program package. In this framework, application of the seminumerical scheme to local hybrid functionals has been discussed, showing preliminary results for the non-self-consistent Lh energy functional.[24]

Here, we provide the first full seminumerical implementation of the self-consistent Lh potential and show that it performs comparably to existing seminumerical global hybrid implementations in terms of calculation time and grid-size dependence. This is the first part of a general implementation of local hybrid functionals into the TURBOMOLE program package that we currently extend to molecular gradients, TDDFT, and other properties. Other exchange-correlation functionals besides Lhs, that employ the exact-exchange energy density as a variable,[25−27] should also benefit from this scheme, for example, the local range-separation approach mentioned above.

THEORETICAL BACKGROUND AND METHODOLOGY

In the GKS scheme, the exchange-correlation potential is defined as a functional derivative of the exchange correlation energy with respect to the molecular orbitals $\{\varphi_i(\mathbf{r})\}$. More specifically, the local hybrid potential referred to in this work is given as

$$\hat{v}_{\mathrm{XC}}^{\mathrm{Lh}}\varphi_i(\mathbf{r}) = \frac{1}{2}\frac{\delta E_{\mathrm{XC}}^{\mathrm{Lh}}}{\delta \varphi_i} \tag{3}$$

Note that the resulting potential is nonlocal and nonmultiplicative due to exact-exchange contributions and should not be confused with the localized, optimized effective potential for global hybrids that has been denoted local hybrid potential in some previous work.[28−30] A detailed and complete derivation of the local hybrid potential defined above can be found in ref 19. While the full expression from eq 3 has been implemented in TURBOMOLE, we will focus on new equations arising in the seminumerical treatment of local hybrid functionals and of the associated potential. For brevity, we will formulate only the closed-shell case throughout this article, keeping in mind that the corresponding open-shell expression is simply the sum over α and β spin contributions.

After summarizing the seminumerical scheme for exact exchange, as used in the ORCA and TURBOMOLE programs, the seminumerical algorithm for the local hybrid potential will be derived and discussed. The RI approximation to the local hybrid potential has also been implemented in TURBOMOLE, and the key aspects of this algorithm will be summarized shortly.

Seminumerical Calculation of Exact Exchange. In many electronic-structure programs, the overall scaling and, for most applications, the total cost of a DFT calculation with global hybrid functionals is dominated by evaluation of the exact-exchange part of the energy and the Kohn−Sham potential.

The basic quantity for the exact-exchange contributions in the GKS scheme is an exchange matrix, which can be defined as the exact-exchange potential $\hat{v}_{\mathrm{X}}^{\mathrm{ex}}$ in the atomic-orbital basis $\{\chi_\mu\}$

$$\begin{aligned} K_{\mu\nu} &= \int \chi_\mu(\mathbf{r})\hat{v}_{\mathrm{X}}^{\mathrm{ex}}\chi_\nu(\mathbf{r})\,\mathrm{d}\mathbf{r} \\ &= \sum_{\kappa\tau} D_{\kappa\tau}\int\int r_{12}^{-1}\chi_\mu(\mathbf{r}_1)\chi_\nu(\mathbf{r}_2)\chi_\kappa(\mathbf{r}_1)\chi_\tau(\mathbf{r}_2)\,\mathrm{d}\mathbf{r}_1\,\mathrm{d}\mathbf{r}_2 \end{aligned} \tag{4}$$

where $\mathbf{D}$ denotes the density matrix.

Given the exchange matrix, the exact-exchange energy is obtained by

$$E_{\mathrm{X}}^{\mathrm{exact}} = -\frac{1}{2}\sum_{\mu\nu} K_{\mu\nu}D_{\mu\nu} \tag{5}$$

Other than efficient analytical integration and prescreening techniques[31] or RI-methods,[32] the computational cost and formal N^4 scaling of the exchange integrals in eq 4 with respect to the basis-set size can be reduced using seminumerical methods. This means that one of the integrations in eq 4 is performed numerically while evaluating analytical Coulomb integrals over two basis functions at each grid point. Pseudospectral algorithms, for instance, allow for particularly accurate results with small grids by employing a specifically designed set of quadrature weights.[21] The COSX algorithm of the Neese group, as implemented in ORCA, and the seminumerical implementation of exact exchange in TURBOMOLE rely exclusively on rigorous prescreening with the overlap and density matrix and may be viewed as a simplified pseudospectral algorithm without use of specialized grids.

In a seminumerical scheme, the exact-exchange matrix element is given by

$$K_{\mu\nu} \approx \sum_{\mathrm{g}}\sum_{\kappa\tau} D_{\kappa\tau}\, X_{\mu\mathrm{g}}X_{\kappa\mathrm{g}}A_{\tau\nu\mathrm{g}} \tag{6}$$

where the basis functions are contracted with the grid-point weights w defining

$$X_{\mu\mathrm{g}} = \chi_\mu(\mathbf{r}_\mathrm{g})\sqrt{w(\mathbf{r}_\mathrm{g})} \tag{7}$$

and the Coulomb integrals over two basis functions

$$A_{\nu\tau\mathrm{g}} = \int \frac{\chi_\nu(\mathbf{r}')\chi_\tau(\mathbf{r}')}{|\mathbf{r}_\mathrm{g} - \mathbf{r}'|}\,\mathrm{d}\mathbf{r}' \tag{8}$$

are calculated analytically at each grid point $\mathbf{r}_\mathrm{g}$.

Evaluation of these integrals represents the bottleneck in this procedure, and their number can be reduced by prescreening

DOI: 10.1021/ct501137x
J. Chem. Theory Comput. 2015, 11, 1540−1548

with the density matrix (P-junctions) and by the overlap between two basis functions (S-junctions). In fact, S-junctions are established between two shells, each consisting of $(2l + 1)$ basis functions that share the same radial part. Coulomb integrals for entire shell pairs that are not connected via an S-junction can be neglected. If a basis function pair $\nu\tau$ is not connected to any other basis function via the density matrix, then the corresponding Coulomb integral does not contribute to the exchange matrix either. Application of these P-junctions is best explained in a stepwise procedure.

In the first step, the density matrix is multiplied with the basis functions, considering only those contributing to a batch of grid points.

$$F_{\tau g} = \sum_{\kappa} D_{\tau\kappa} X_{\kappa g} \tag{9}$$

Subsequently, the Coulomb integrals (eq 8) are computed and immediately contracted with the **F** matrix, giving

$$G_{\nu g} = \sum_{\tau} F_{\tau g} A_{\nu\tau g} \tag{10}$$

Some analytical integrals $A_{\nu\tau g}$ can be neglected for the entire batch of grid points if the matrix **F** exhibits zero rows. Following from the definition, this is due to a combination of neglected basis functions on a batch of grid points, small weights (see eq 7), and negligible density-matrix elements.

Finally, the summation within each batch of grid points is the product between the two matrices **X** and **G**

$$K_{\mu\nu} = \sum_{g} X_{\mu g} G_{\nu g} \tag{11}$$

Since the exchange matrix is linear in the density matrix, it can be calculated from the difference between the density matrix in a given iteration and previous density matrices. The full exact-exchange contribution is subsequently reassembled from exchange matrices of the current and previous iterations. Prescreening with the difference-density matrix reduces the number of P-junctions substantially toward convergence. While this procedure formally scales quadratically with the number of basis functions and linearly with the number of grid points, an overall linear scaling with system size (going to large molecules) has been claimed for COSX.[22]

The Seminumerical Local Hybrid Potential. The exact-exchange energy density employed in local hybrids and other modern density functionals is given in terms of the density matrix **D** and the atomic basis functions $\{\chi_\mu\}$

$$\varepsilon_X^{ex}(\mathbf{r}) = -\frac{1}{2} \sum_{\mu\nu\kappa\tau} D_{\kappa\tau} D_{\mu\nu} \chi_\mu(\mathbf{r})\, \chi_\kappa(\mathbf{r}) \int \frac{\chi_\nu(\mathbf{r}')\, \chi_\tau(\mathbf{r}')}{|\mathbf{r} - \mathbf{r}'|}\, d\mathbf{r}' \tag{12}$$

If the LMF in a local hybrid functional is a semilocal quantity, then only the first term in eq 2 contains exact exchange and needs to be considered for the seminumerical scheme. The second exchange term, as well as the correlation functional, are semilocal functionals. Their contribution to the exchange-correlation energy and potential can be implemented straightforwardly following the usual procedures for this type of functionals.

From the first term in the Lh exchange energy (eq 2)

$$\tilde{E}_X^{ex} = \int a(\mathbf{r})\, \varepsilon_X^{ex}(\mathbf{r})\, d\mathbf{r} \tag{13}$$

two different contributions to the GKS potential arise: a nonlocal part that is due to the derivative of the exact-exchange energy density and a local contribution exhibiting derivatives of the LMF multiplied with the exact-exchange energy density. Assuming an LMF that depends on common meta-GGA ingredients, i.e., the density ρ, the square of the density gradient $\gamma(\mathbf{r}) = |\nabla\rho(\mathbf{r})|^2$, and the kinetic energy density τ, the following $\varepsilon_X^{ex}(\mathbf{r})$-dependent potential terms expressed in the atomic basis set emerge

$$\begin{aligned}
\tilde{K}^{\rho}_{\mu\nu} &= \int \varepsilon_X^{ex}(\mathbf{r})\, \frac{\partial a(\mathbf{r})}{\partial \rho(\mathbf{r})}\, \chi_\mu(\mathbf{r})\, \chi_\nu(\mathbf{r})\, d\mathbf{r} \\
\tilde{K}^{\gamma}_{\mu\nu} &= \int \varepsilon_X^{ex}(\mathbf{r})\, \frac{\partial a(\mathbf{r})}{\partial \gamma(\mathbf{r})} \nabla\rho(\mathbf{r})\cdot\nabla(\chi_\mu(\mathbf{r})\, \chi_\nu(\mathbf{r}))\, d\mathbf{r} \\
\tilde{K}^{\tau}_{\mu\nu} &= \int \varepsilon_X^{ex}(\mathbf{r}) \nabla\chi_\mu(\mathbf{r})\cdot\nabla\chi_\nu(\mathbf{r})\, \frac{\partial a(\mathbf{r})}{\partial \tau(\mathbf{r})}\, d\mathbf{r}
\end{aligned} \tag{14}$$

In order to perform the integration in eqs 13 and 14, numerically, the exact-exchange energy density is required at each grid point $\mathbf{r}_g$. It is given in terms of the quantities defined in the previous section as follows

$$\varepsilon_X^{ex}(\mathbf{r}_g) = -\frac{1}{2} \sum_{\mu\nu\kappa\tau} X_{\mu g} D_{\mu\nu} A_{\nu\tau g} D_{\tau\kappa} X_{\kappa g} = -\frac{1}{2} \sum_{\nu} F_{\nu g} G_{\nu g} \tag{15}$$

Prescreening of the Coulomb integrals is done analogously to the seminumerical treatment of exact exchange in global hybrids, using S- and P-junctions as described above. Note, however, that the exact-exchange energy density depends quadratically on the density matrix. It, therefore, cannot be calculated from a difference-density matrix and subsequently reassembled. In principle, this procedure could be applied to the integrals $G_{\nu g}$ (defined in eq 10), which are linear in the density matrix. However, as the number of grid points (n_g) usually exceeds the number of basis functions (n_{bas}), a much larger number of integrals $(n_{bas} \times n_g)$ would have to be stored as compared to storing the symmetric exchange matrix given in eq 4 (representing $n_{bas}(n_{bas} + 1)/2$ integrals). Attempts in this direction, therefore, have not been made so far. Note that, in particular for medium-sized molecules, prescreening with the full density matrix alone cancels only very few integrals. Instead, only the combined prescreening with the density matrix, maximum values of contributing basis functions on a batch of grid points, and grid-point weights is mandatory. This amounts to directly searching for zero rows in the **F**-matrix.

As pointed out above, an additional nonlocal and non-multiplicative contribution to the potential emerges due to derivatives of the exact-exchange energy density with respect to the orbitals. Defining the modified exchange matrix $\tilde{K}$ as the LMF-weighted exact-exchange operator in the AO basis

$$\tilde{K}_{\mu\nu} = \int \chi_\mu(\mathbf{r})\, a(\mathbf{r})\, \hat{v}_X^{ex} \chi_\nu(\mathbf{r})\, d\mathbf{r} \tag{16}$$

the nonlocal part of the Lh potential is represented by the symmetric part of $\tilde{\tilde{K}}$

$$\begin{aligned}
&-\frac{1}{2}\left(\int a(\mathbf{r})\, \chi_\mu(\mathbf{r})\, \hat{v}_X^{ex} \chi_\nu(\mathbf{r})\, d\mathbf{r} + \int \chi_\mu(\mathbf{r})\, \hat{v}_X^{ex}(a(\mathbf{r})\, \chi_\nu(\mathbf{r}))\, d\mathbf{r}\right) \\
&\quad = -\frac{1}{2}(\tilde{K}_{\mu\nu} + \tilde{K}_{\nu\mu})
\end{aligned} \tag{17}$$

DOI: 10.1021/ct501137x
J. Chem. Theory Comput. 2015, 11, 1540−1548

In the seminumerical scheme, this integral is readily obtained by inserting the LMF into the expression for the seminumerical exact-exchange integral in eq 11

$$\tilde{K}_{\mu\nu} = \sum_{g} a_g X_{\mu g} \sum_{\tau} F_{\tau g} A_{\tau\nu g} = \sum_{g} a_g X_{\mu g} G_{\nu g} \tag{18}$$

Due to the position-dependent weighting of exact exchange through the LMF, integral screening with the LMF seems appealing. To avoid calculation of the **A**-matrix for a whole batch of grid points, the LMF itself as well as all derivatives (cf. eq 14) need to vanish. However, this occurrence is negligible for the LMF and the molecules considered here and thus such a prescreening has not been pursued. The remaining terms in the local hybrid potential[19] arising from the semilocal exchange or correlation energy part (last two terms in eq 2) are purely local and multiplicative. Their implementation is equivalent to any semilocal density functional and needs no further discussion.

RI Approximation to the Local Hybrid Potential. In the framework of the localized Hartee−Fock approximation[17] to the optimized effective potential, it has been suggested that the Slater potential can be approximated using an RI. Since the exact-exchange energy density is proportional to the Slater potential, this approach has been adapted for the implementation of local hybrid functionals.[18,19] The RI or completeness insertion corresponds in both cases to fitting the exact-exchange potential to the atomic-orbital basis set

$$\begin{aligned}\hat{v}_X^{ex}\chi_\mu(\mathbf{r}) &= \sum_{\kappa\tau} D_{\kappa\tau} \int \frac{\chi_\kappa(\mathbf{r}')\,\chi_\mu(\mathbf{r}')}{|\mathbf{r}-\mathbf{r}'|}\,d\mathbf{r}'\chi_\tau(\mathbf{r}) \\ &= \sum_{\nu} d_{\mu\nu}\chi_\nu(\mathbf{r})\end{aligned} \tag{19}$$

and enforcing the overlap norm to calculate the fitting coefficients $d_{\mu\nu}$.

Consequently, the exact-exchange potential acting on a basis function χ_μ can be expressed in terms of the exchange (eq 4) and the overlap matrix **S**

$$\hat{v}_X^{ex}\chi_\mu(\mathbf{r}) = \sum_{\kappa\tau} \chi_\kappa(\mathbf{r})\, S^{-1}_{\kappa\tau} K_{\tau\mu} \tag{20}$$

Inserting this expression into the relation between the exact-exchange potential and the exact-exchange energy density

$$\varepsilon_X^{ex}(\mathbf{r}) = -\frac{1}{2}\sum_{\mu\nu} \chi_\mu(\mathbf{r})\, \hat{v}_X^{ex}\chi_\nu(\mathbf{r}) \tag{21}$$

gives an RI approximation to the exact-exchange energy density

$$\varepsilon_X^{ex}(\mathbf{r}) = Tr(X(\mathbf{r})\, S^{-1} K D) \tag{22}$$

where the matrix **X** contains products of basis functions

$$X_{\mu\nu} = \chi_\mu(\mathbf{r})\,\chi_\nu(\mathbf{r}) \tag{23}$$

Likewise, an analytical expression for the LMF-weighted exact-exchange integral is obtained by combining the RI approximation to the exact-exchange potential (eq 20) with eq 16

$$\tilde{K}_{\mu\nu} = \sum_{\kappa,\tau} L_{\mu\kappa} S^{-1}_{\kappa\tau} K_{\tau\nu} \tag{24}$$

where the LMF matrix

$$L_{\mu\nu} = \int \chi_\mu(\mathbf{r})\, a(\mathbf{r})\, \chi_\nu(\mathbf{r})\, d\mathbf{r} \tag{25}$$

is calculated on a grid together with the other DFT integrals without affecting the overall costs.

Following our former procedure for localized local hybrid potentials,[19] the RI approximation has been applied *after* deriving the Lh potential as a functional derivative with respect to the orbitals. In another GKS implementation of local hybrid functionals,[18] the RI was applied first to the energy expression, subsequently taking the derivative with respect to the orbitals. As a result, the potentials differ slightly. The difference can be recovered if, in our approach, the RI is inserted once between the LMF and the exact-exchange potential and once between a basis function and the LMF in eq 17. This corresponds to fitting the LMF and the exact-exchange potential with the same (auxiliary) basis set.

Investigation of the differences in the resulting potentials is beyond the scope if this work, and there are two caveats that render both approaches impractical: (i) the basis-set expansion does not yield the correct asymptotic behavior for the potential and (ii) rather large and weakly contracted basis sets of high quality are needed.[33] The second issue will be addressed in more detail below.

One solution to the basis-set problem would be the introduction of dedicated auxiliary basis sets. This procedure leads, however, to unsymmetric four-center Coulomb integrals over three atomic and one auxiliary basis function. The lack of symmetry and the usually larger size of the auxiliary basis set would increase the computational cost considerably. Furthermore, the exact-exchange energy density and potential have to be calculated numerically in the small-density regions outside the molecule in order to retain the correct asymptotics.

Computational Details. Local hybrid functionals have been implemented into a development version of the TURBOMOLE program package.[34] The RI approximation and, for comparison, an initial numerically accurate but inefficient seminumerical implementation of the potential were included in the dscf module.[35] By comparing RI results with seminumerical calculations from the dscf module (using large grids and no prescreening), the accuracy of the RI approximation to the local hybrid potential is studied. The efficient version of the seminumerical local hybrid potential presented in this work has been implemented into the ridft module.[36] This module uses an RI-approximation to the Coulomb energy and is, at least for semilocal functionals, usually faster than the dscf module. All calculations assessing accuracy and timing of the seminumerical local hybrid potential, as well as comparisons with the TPSSh functionals, are therefore run with the ridft module.

Unless stated otherwise, TZVP basis sets have been used for energy calculations[37] and the IGLO-IV[38] basis for isotropic hyperfine coupling constants (HFCCs). Additionally, the SVP[39] and QZVP[40] basis sets and the smaller IGLO-II and IGLO-III basis sets[38] have been employed for total energies and isotropic HFCCS, respectively. In the ridft module, the default auxiliary basis sets for the RI Coulomb integrals have been taken (TZVP[41] and universal[42] sets, respectively). For the G2-1[43,44] set of molecules, MP2 structures have been taken from refs 43 and 44. The isotropic HFCCs of 13 small organic molecules have been calculated at experimental structures[45] using the MAG-ReSpect program.[46] Structures for cholesterol and vancomycin are taken from a larger test set in ref 22. A representative Lh functional based on Slater exchange[47,48] and VWN correlation[49] together with a scaled t-LMF[50]

DOI: 10.1021/ct501137x
J. Chem. Theory Comput. 2015, 11, 1540−1548

$$a(\mathbf{r}) = 0.5t(\mathbf{r}) = 0.5\frac{\tau_W(\mathbf{r})}{\tau(\mathbf{r})} \quad (26)$$

defined as the ratio between the von Weizsäcker kinetic-energy density τ_W and the kinetic-energy density τ, has been used. All timing evaluations are performed on a single core of an Intel Core 3.40 GHz i3-4130 processor.

EFFICIENCY AND ACCURACY

Global hybrid functionals can be seen as a special, simplified case of the more general local hybrid scheme, where a constant LMF is inserted. Seminumerical implementations for global hybrids within the pseudospectral or COSX frameworks have been discussed in some detail previously, in comparison with fully analytical calculations of the exact-exchange four-center integrals or with an RI approximation[32] to exact exchange.[51] It has been shown clearly that (i) seminumerical exact exchange does not require larger grids than that needed for the semilocal ingredients of global hybrids and (ii) the formally lower basis-set scaling of seminumerical compared to fully analytical exact exchange favors the use of the seminumerical schemes for very large systems. The crossover with increasing system size may, however, depend appreciably on details of the implementation and in particular on the efficiency of the analytical two-electron integral code. For the present purpose of providing the self-consistent Lh potential at comparable cost to global hybrids in terms of scaling and prefactor, it will thus be sufficient to focus on the comparison of seminumerical treatments for global and local hybrids. That is, we need to show that the additional aspects that distinguish local from global hybrids will not notably affect the efficiency of the implementation. Then more elaborate procedures to reduce the computational cost of exact exchange are expected to apply also to local hybrids. This holds for various strategies of reducing the necessary grid sizes, refining prescreening,[52] and improving error cancellations (e.g., ref 53) as well as for possible extensions to periodic boundary conditions.[54] We will nevertheless also provide timing comparisons to the very efficient analytical treatment of exact exchange in the ridft module of Turbomole.

To assess the accuracy of the seminumerical Lh potential, the convergence of total energies and of isotropic hyperfine coupling constants (HFCC) with grid size will be discussed. While the procedure scales linearly with grid size, the number of grid points is generally much larger than the number of basis functions. For molecules with less than 100 atoms and medium-size basis sets, the grid size therefore has a rather large impact on the computational cost and should be chosen to be as small as possible. Since no analytically exact data are available for Lh calculations, seminumerical results with the large grids (grid size 6 or 7 in Turbomole) will serve as a reference. For comparison, the basis-set dependence of the RI approximation for Lh functionals will be discussed as well.

Finally, the efficiency of our Lh implementation is tested against calculations with the TPSSh hybrid functional, since it contains the same basic quantities (density, gradient of the density, kinetic energy density, and exact exchange). Both the senex and the analytical integration scheme (ex-K) for exact exchange in the ridft module are considered as references for the computational cost.

Accuracy for Total Energies. The convergence of total energies for the atoms and molecules of the small G2-1 set is illustrated in Figures 1 and 2. Figure 1 confirms previous claims that large uncontracted basis sets are needed for the RI approximation. Decontracting the basis improves the total energies to a much larger extent than that using contracted basis sets with higher maximal angular momentum. Rather large errors of more than 0.1 hartree are obtained with all contracted basis sets. For the lithium atom, the energy could not be converged with SVP basis due to unphysical values for the potential in the asymptotic region. The requirement of the mean and maximum absolute deviation to be below 1 mHartree is met only by the uncontracted QZVP basis. This exemplifies why local hybrids so far have been considered to be significantly more expensive than global hybrid functionals.

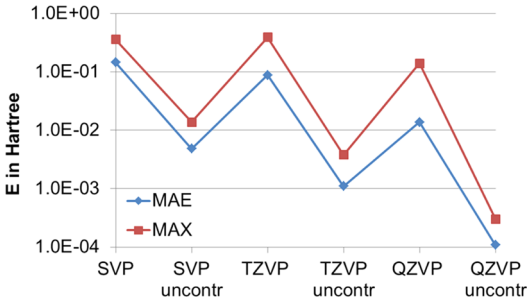

Figure 1. Difference in total energies (in hartree) between the RI approximation and the seminumerical implementation with large grid (size 6 in Turbomole) for different basis sets. The mean and maximum absolute error for 11 atoms and 55 molecules in the G2-1 set are shown. Due to convergence problems for small basis sets with the RI approach, the lithium atom has been omitted.

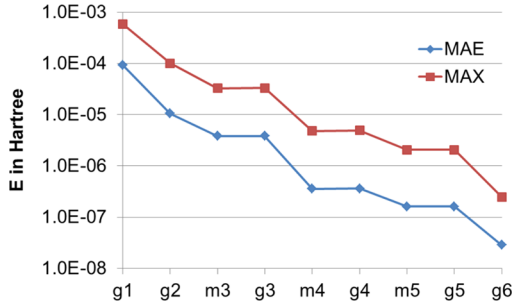

Figure 2. Seminumerical implementation: deviation of total energies (in hartree) from results with large grid (grid size 7) for different grid sizes as defined in Turbomole. The mean and maximum error for 12 atoms and 55 molecules of the G2-1 set are shown.

Using even the smallest grid, the seminumerical scheme is more accurate than the RI approximation with the uncontracted QZVP basis (Figure 2). For the m3 grid, which is commonly used for DFT calculations with Turbomole, a maximum error of 32 μHartree for the G2-1 set is obtained. This value is in the range of errors of the RI approximation for the Coulomb term and certainly much smaller than errors of typical functionals for relative energies. The standard m3 grid can therefore be recommended for Lh calculations as well.

Accuracy for Isotropic Hyperfine Coupling Constants. The total energy and related quantities such as atomization energies and reaction barriers are usually well-approximated with so-called modified grids. This means that smaller grids are used for the self-consistent-field (SCF) iterations, and the final energy is evaluated with a larger grid. As other properties may feature different sensitivity to the grid, an evaluation for properties seems to be important. We have chosen here to look at isotropic HFCCs, as these are determined by the spin density at the nucleus and they are known to be affected also by subtle

DOI: 10.1021/ct501137x
J. Chem. Theory Comput. 2015, 11, 1540−1548

spin-polarization effects in the core shells. Dependence of a set of HFCCs for 13 small main-group molecules (overall 36 values) on the basis set for the RI approximation is evaluated in Figure 3, whereas the influence of grid size in the semi-numerical scheme is considered in Figure 4. With the commonly used IGLO basis sets, the maximum error of the RI approximation ranges from more than 40% with the IGLO-II basis to roughly 5% with the decontracted IGLO-IV basis. The mean absolute errors are in the range of 0.5 and 8%. Note that, compared to the energies above, the effect of decontraction is less pronounced due to the already loosely contracted nature of these basis sets. Decontraction of the IGLO-III basis actually increases both the MAE and the maximum absolute error somewhat. This suggests poor convergence of the RI approximation with the atomic-orbital basis set and possibly some error compensation for the smaller basis sets. Overall, it is evident that the basis set must be chosen very carefully if the RI approximation is used for local hybrid functionals in the calculation of such properties.

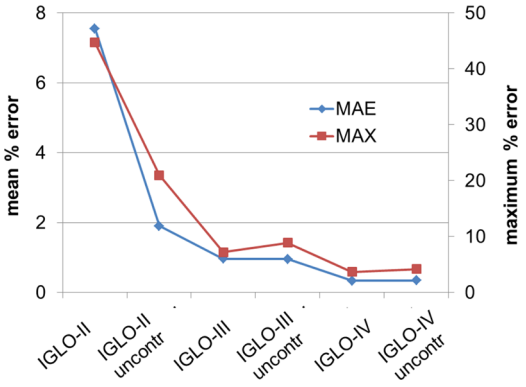

Figure 3. Difference between the RI approximation and the seminumerical implementation (for grid size 6 in Turbomole) for isotropic hyperfine coupling constants using different basis sets. The mean and maximum absolute percentage error for 36 isotropic HFCCs of 13 small main-group molecules are shown.

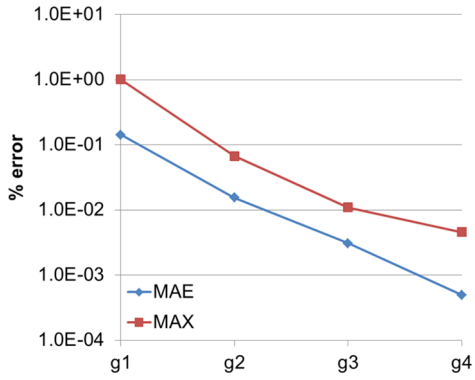

Figure 4. Convergence of 36 isotropic hyperfine coupling constants for 13 small main-group compounds with grid size using the seminumerical implementation (IGLO-IV basis results). The mean and maximum absolute percentage error with respect to a large grid (size 7 in Turbomole) are shown.

In the seminumerical scheme, convergence of the isotropic hyperfine coupling constants with grid size is excellent (Figure 4). Since the isotropic hyperfine coupling constant is only given with an accuray of 0.01 MHz, only results up to grid size 4 are shown. The maximum error of about 1% with the smallest grid (size 1) is obtained for the fluorine atom in the FCl^- anion. With the given test set, the maximum error of 0.01% for grid size 3 represents an acceptable accuracy of 0.1 MHz. Such a grid is already recommended for semilocal functionals. That is, even for the sensitive HFCCs, the grid requirements for local hybrids are comparable to those needed for standard functionals.

Timing. We note that for senex, analytical exact exchange, and the present local hybrid implementation in the ridft module of Turbomole the RI approximation is generally used for the Coulomb integrals, which renders the Coulomb contributions unimportant for the overall timing. Figure 5 shows the scaling of the seminumerical implementation of the Lh potential for carbon chains. The time per SCF cycle for a local hybrid is compared to a calculation with the TPSSh global hybrid using the senex algorithm. For comparison, timing for the TPSSh analytical implementation of exact exchange in the ridft module is also provided. Within the seminumerical scheme, the timing for the local and global hybrid is almost identical. Construction of the analytical one-electron integrals (eq 8) on the grid is the most time-consuming step of the exact-exchange computation, and calculation of the additional terms occurring in the Lh potential, and not in the global hybrid, is negligible. As mentioned earlier, and already pointed out in ref 24, the

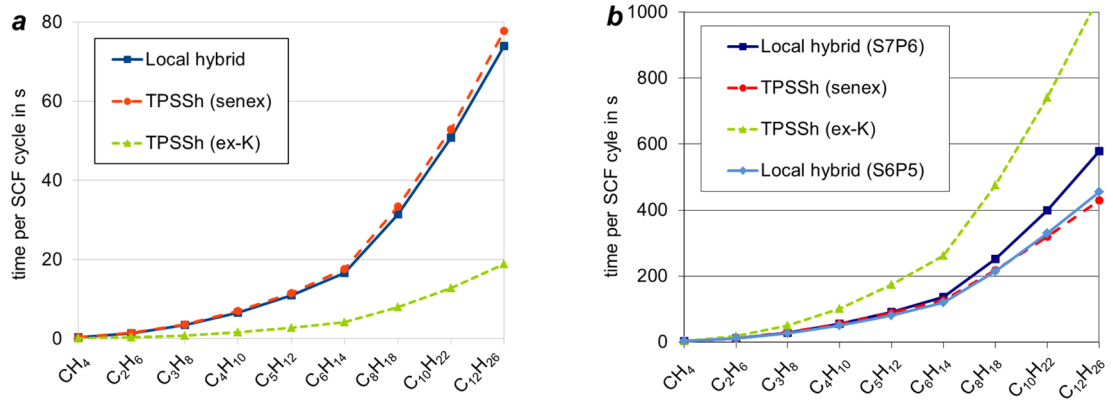

Figure 5. Time per SCF cycle for carbon chains (grid size 1; (a) TZVP and (b) QZVP basis) comparing calculations with a local hybrid functional and the TPSSh global hybrid using the seminumerical (senex) and analytical (ex-K) implementation of exact exchange in the ridft module. Two sets of thresholds for S- and P-junctions are considered, with the corresponding exponents in parentheses.

DOI: 10.1021/ct501137x
J. Chem. Theory Comput. 2015, 11, 1540−1548

analytical implementation is faster for small systems, medium-size basis sets, and even the smallest Turbomole grid. To reduce computational cost, smaller grids have been designed for the senex scheme. Since we have not attempted to devise specialized grids but used standard settings for a DFT calculation, i.e., gridsize m3 (grid size 1 for the iterations), the analytical implementation of exact exchange in the ridft module of Turbomole, which is known to be extremely efficient, is still faster for the carbon chains considered, i.e., up to $C_{12}H_{26}$, when using TZVP basis sets. Turning, however, to larger QZVP basis sets (Figure 5b) already reverts the situation: now the seminumerical treatments are more efficient due to their better basis-set scaling behavior (see above). The figure also shows that the performance of the seminumerical treatment depends on the settings chosen for the S- and P-junctions. While the local hybrid calculations are still slower than senex calculations with TPSSh (and default settings) upon use of conservative settings (S-junctions 10^{-7}, P-junctions 10^{-6}), increasing the thresholds to 10^{-6} and 10^{-5}, respectively, makes the computation times of the two seminumerical implementations essentially equal.

In full SCF procedures, the density matrix of a given iteration may be decomposed into a linear combination of the previous density matrix and a remaining difference-density matrix. Since the exchange matrix (eq 4) is linear in the density matrix, it can be calculated using the difference-density matrix and subsequently combined with the previous exchange matrices to the full exact-exchange contribution. Integral prescreening with the difference-density matrix is done for analytical[35] as well as seminumerical exact exchange (COSX and senex), effectively accelerating the entire calculation. As indicated above, such a use of the difference-density matrix is not possible with local hybrids. Table 1 contains timing for the full SCF procedure

Table 1. Timing (in Seconds) for the Full SCF Procedure with the Ridft Module of TURBOMOLE Comparing a Local Hybrid Functional to the TPSSh Functional Using the Seminumerical (senex) or Analytical (ex-K) Implementation of Exact Exchange[a]

	local hybrid	TPSSh senex	TPSSh senex[b]	TPSSh ex-K	TPSSh ex-K[b]
CH_4	3.2 (6)	3.0 (5)	3.1 (5)	0.4	0.5
C_2H_6	13.1 (6)	14.0 (6)	13.6 (6)	1.8	1.6
C_3H_8	36.2 (7)	35.3 (6)	35.3 (6)	4.8	4.1
C_4H_{10}	70.1 (7)	68.1 (6)	68.4 (6)	10.0	7.8
C_5H_{12}	117.3 (7)	113.0 (6)	112.5 (6)	17.2	12.9
C_6H_{14}	178.0 (7)	170.3 (6)	166.8 (6)	26.8	19.2
C_8H_{18}	338.6 (7)	324.1 (6)	313.1 (6)	50.0	34.9
$C_{10}H_{22}$	547.8 (7)	512.9 (6)	489.3 (6)	80.2	53.9
$C_{12}H_{26}$	804.1 (7)	819.0 (7)	755.1 (7)	134.6	83.3

[a]TZVP basis sets and grid size m3 have been employed. The number of iterations is given in parentheses. B3LYP orbitals were used as an initial guess. [b]With difference-density matrix algorithm.

with a local hybrid and with TPSSh using either senex or the analytical exact exchange. With increasing molecule size, prescreening with the difference-density matrix algorithm becomes more important, and the maximal timing reduction for $C_{12}H_{26}$ is 64 s, representing less than 10% of the total computational cost. Within the seminumerical scheme, the timing for the full SCF procedure with local hybrid functionals is equal or, with the difference-density matrix algorithm switched on, at least comparable to the global hybrid calculation. For the systems considered in Table 1, calculations with the analytical exact-exchange treatment of the ridft module are faster overall than senex or local hybrid calculations. Note that this type of still relatively small chain-like molecules in combination with moderate basis sets (TZVP) represents a worst-case scenario for the seminumerical scheme, whereas the highly efficient analytical scheme can benefit maximally from integral prescreening. As expected, analytical exact exchange becomes less advantageous with increasing chain length (from a factor 8 for CH_4 through 6 for $C_{12}H_{26}$) without the difference-density matrix algorithm. Use of the difference-density matrix algorithm reverses the increased speed of ex-K as compared to both the local and global hybrid calculations in the seminumerical scheme with increasing system size. As shown earlier for seminumerical Hartree−Fock or global hybrid schemes,[21,22,24,53] this will change for more three-dimensional molecules and with increasing molecule and basis-set size. The last claim is strongly supported by the comparative timing for the TZVP and QZVP basis sets in Figure 5, which shows clearly that with the larger basis set both seminumerical algorithms outperform the analytical treatment.

Additionally, the influence of screening via S- and P-junctions increases with molecular size. As an example, timing for cholesterol with different thresholds is given in Table 2. The

Table 2. Timing of the Full SCF Procedure for Cholesterol (74 Atoms, 836 Basis Functions) with a Local Hybrid and the TPSSh Functional Using the Seminumerical (senex) or Analytical (ex-K) Scheme[a]

	thresholds for junctions				
	S	P	difference density matrix	t_{ridft} (s)	ΔE in μHartree
local hybrid	10^{-5}	10^{-5}		4471.5	11.95
local hybrid	10^{-6}	10^{-5}		4869.7	9.05
local hybrid	10^{-7}	10^{-5}		5133.5	9.23
local hybrid	10^{-7}	10^{-6}		6181.7	0.00426
TPSSh(senex)	default		yes	5263.0	
TPSSh(senex)	default		no	5796.6	
TPSSh(ex-K)			yes	862	
TPSSh(ex-K)			no	1547.4	

[a]Different thresholds for P- and S-junctions are considered. The accuracy with respect to a calculation without prescreening is given as ΔE. B3LYP start orbitals, TZVP basis sets, and the m3 grid were used. Convergence was always reached after 8 iterations.

computation time for a local hybrid functional with conservative thresholds (10^{-6} for P- and 10^{-7} for S-junctions) is slightly higher than the time for a global hybrid functional using the senex algorithm. It is, however, possible to reduce the computational cost considerably by tuning the thresholds. Aiming for efficiency, the error of 11.95 μHartree with S- and P-junctions of 10^{-5} is certainly still acceptable. With these settings, the final computation time is faster than the TPSSh calculation with the senex scheme employing the difference-density matrix algorithm. Compared to the analytical implementation of exact exchange in the ridft module, the local hybrid calculation is slower by a factor 5.2 with or 2.9 without the difference-density matrix algorithm. With the same settings and TZVP basis sets, these factors decrease to 4.6 and 2.1, respectively, for the larger vancomycin molecule (Table 3).

DOI: 10.1021/ct501137x
J. Chem. Theory Comput. 2015, 11, 1540−1548

Table 3. Timing of the Full SCF Procedure for Vancomycin (176 Atoms, 2476 Basis Functions) with a Local Hybrid and the TPSSh Functional Using the Analytical Implementation of Exact Exchange[a]

	t_{ridft} (s)	SCF cycles
local hybrid	39 932	10
tpssh	19 224	11
tpssh[b]	8604	11

[a]Thresholds for S- and P-junctions in the local hybrid calculation are 10^{-5}. B3LYP start orbitals, TZVP basis sets, and the m3 grid were used. [b]With difference-density matrix algorithm.

It is thus expected that the computational cost of local hybrid functionals becomes less than or equal to that of global hybrid functionals with analytical exact exchange as we go to large, more globular molecules and in particular to large basis sets.

The cholesterol and vancomycin examples have been used previously to evaluate the COSX seminumerical algorithm in ORCA (for Hartree−Fock and global hybrid calculations). In that case, increased speed compared to the underlying analytical algorithms (standard direct SCF procedure in ORCA) was found. As previous comparisons of the Turbomole senex and ORCA COSX algorithms already indicated comparable performance, the lack of a significant increase in speed in the present Turbomole comparisons thus attests to the high efficiency of the analytical scheme in the ridft module (compared to the analytical scheme used in ref 22) rather than to an inefficiency of the seminumerical implementation. It has also been shown that with larger QZVP basis sets[24] the senex scheme was already slightly faster than analytical exact exchange for cholesterol. The crossover between seminumerical and analytical schemes is sensitive not only to the basis sets but also, of course, to grid sizes and other parameters inherent to both seminumerical and analytical implementations. The main result of the present timing comparisons is that the seminumerical implementation of local hybrids requires very little extra computational effort compared to global hybrids, even though the difference-density matrix algorithm can be applied only to the latter. Indeed, evaluation of the exact-exchange energy density and nonlocal terms in the local hybrid potential represents roughly 90% of the total computation time due to the underlying two-center Coulomb integrals to be computed on the grid. This procedure, therefore, should be transferable to other functionals based on the exact-exchange energy density without significant loss of efficiency.

CONCLUSIONS

Seminumerical treatments of exact exchange have been shown here to be particularly well-suited for an efficient self-consistent implementation of local hybrid functionals. The use of RI approximations for the nonstandard two-electron integrals occurring in previous self-consistent implementations of local hybrids could thus be circumvented. While those RI-based implementations need very large, uncontracted basis sets, rendering the calculations inefficient, the present seminumerical scheme has no particular basis-set requirements beyond those of standard Kohn−Sham schemes, and it is numerically accurate with standard DFT grids. The extra computational costs for terms specific to the local hybrid potential are only a relatively small fraction of the computing time needed to evaluate the exact-exchange parts. Within this framework, local hybrids thus require comparable computational effort as that of global ones. As the seminumerical integration becomes most efficient for large systems and large basis sets, self-consistent calculations with local hybrids are now accessible for any system for which one may apply global hybrids. Other approaches to improve the efficiency of calculations with exact exchange should also apply to local hybrids. Additionally, a straightforward parallelization over batches of grid points can be realized for the present local hybrid implementation. Judging from the timing discussed above, the increase in speed is expected to be similar to the favorable behavior reported for the COSX algorithm. In fact, any other density functional approximation that relies on the exact-exchange energy density will also benefit from the efficient evaluation of this quantity. The seminumerical implementation discussed in this work should thus allow for a broader application range of many other classes of hyper-GGA-type functionals as well. In recent years, hybrid functionals have become increasingly popular in solid-state physics and materials science. With local hybrid functionals, very different physical areas such as surfaces or impurities could be distinguished from more homogeneous regions. Additionally, exact-exchange screening or long-range correction can be included as a modification of our method. Seminumerical schemes comparable to the one evaluated here may thus offer ways to efficiently implement even more sophisticated functionals for extended systems also.

AUTHOR INFORMATION

Corresponding Author

*E-mail: hilke.bahmann@tu-berlin.de.

Notes

The authors declare no competing financial interest.

ACKNOWLEDGMENTS

We are grateful to the Turbomole developers consortium for access to the development version, as well as for helpful discussions, in particular with Florian Weigend, at the developers meetings.

REFERENCES

(1) Becke, A. D. *J. Chem. Phys.* **1993**, *98*, 1372.
(2) Becke, A. D. *J. Chem. Phys.* **1997**, *107*, 8554.
(3) Perdew, J. P.; Ernzerhof, M.; Burke, K. *J. Chem. Phys.* **1996**, *105*, 9982.
(4) Zhao, Y.; Truhlar, D. G. *Theor. Chem. Acc.* **2008**, *120*, 215.
(5) Heyd, J.; Scuseria, G. E.; Ernzerhof, M. *J. Chem. Phys.* **2003**, *118*, 8207.
(6) Yanai, T.; Tew, D.; Handy, N. *Chem. Phys. Lett.* **2004**, *393*, 51.
(7) Jaramillo, J.; Scuseria, G. E.; Ernzerhof, M. *J. Chem. Phys.* **2003**, *118*, 1068.
(8) Perdew, J. P.; Staroverov, V. N.; Tao, J.; Scuseria, G. E. *Phys. Rev. A* **2008**, *78*, 052513.
(9) Schmidt, T.; Kraisler, E.; Makmal, A.; Kronik, L.; Kümmel, S. *J. Chem. Phys.* **2014**, *140*, 18A510.
(10) Arbuznikov, A. V.; Kaupp, M. *J. Chem. Phys.* **2008**, *128*, 214107.
(11) Arbuznikov, A. V.; Bahmann, H.; Kaupp, M. *J. Phys. Chem. A* **2009**, *113*, 11898.
(12) Arbuznikov, A. V.; Kaupp, M. *Chem. Phys. Lett.* **2007**, *440*, 160.
(13) Tao, J.; Staroverov, V. N.; Scuseria, G. E.; Perdew, J. P. *Phys. Rev. A* **2008**, *77*, 012509.
(14) Arbuznikov, A. V.; Kaupp, M. *J. Chem. Phys.* **2014**, *141*, 204101.
(15) Haunschild, R.; Scuseria, G. E. *J. Chem. Phys.* **2010**, *132*, 224106.
(16) Henderson, T. M.; Janesko, B. G.; Scuseria, G. E.; Savin, A. *Int. J. Quantum Chem.* **2009**, *109*, 2023.
(17) Della Sala, F.; Görling, A. *J. Chem. Phys.* **2001**, *115*, 5718.

DOI: 10.1021/ct501137x
J. Chem. Theory Comput. 2015, 11, 1540−1548

(18) Janesko, B. G.; Krukau, A. V.; Scuseria, G. E. *J. Chem. Phys.* **2008**, *129*, 124110.
(19) Arbuznikov, A. V.; Kaupp, M.; Bahmann, H. *J. Chem. Phys.* **2006**, *124*, 204102.
(20) Hesselmann, A.; Manby, F. *J. Chem. Phys.* **2005**, *123*, 164116.
(21) Greeley, B. H.; Russo, T. V.; Mainz, D. T.; Friesner, R. A. *J. Chem. Phys.* **1994**, *101*, 4028.
(22) Neese, F.; Wennmohs, F.; Jansen, A.; Becker, U. *Chem. Phys.* **2009**, *356*, 98.
(23) Ahlrichs, R.; Baer, M.; Haeser, M.; Horn, H.; Koelmel, C. *Chem. Phys. Lett.* **1989**, *162*, 165.
(24) Plessow, P.; Weigend, F. *J. Comput. Chem.* **2012**, *33*, 810.
(25) Odashima, M. M.; Capelle, K. *Phys. Rev. A* **2009**, *79*, 062515.
(26) Becke, A. *J. Chem. Phys.* **2005**, *122*, 064101.
(27) Přecechtělová, J.; Bahmann, H.; Kaupp, M.; Ernzerhof, M. *J. Chem. Phys.* **2014**, *141*, 111102.
(28) Arbuznikov, A. V.; Kaupp, M. *Chem. Phys. Lett.* **2004**, 881.
(29) Hieringer, W.; Della Sala, F.; Della Sala, F.; Görling, A. *Chem. Phys. Lett.* **2004**, *383*, 115.
(30) Teale, A. M.; Tozer, D. J. *Chem. Phys. Lett.* **2004**, *383*, 109.
(31) Ochsenfeld, C.; White, C. A.; Head-Gordon, M. *J. Chem. Phys.* **2002**, *109*, 1663.
(32) Weigend, F. *Phys. Chem. Chem. Phys.* **2002**, *4*, 4285.
(33) Della Sala, F.; Görling, A. *J. Chem. Phys.* **2002**, *116*, 5374.
(34) *TURBOMOLE*, V6.6; University of Karlsruhe and Forschungszentrum Karlsruhe GmbH: Karlsruhe, Germany, 2014; http://www.turbomole.com
(35) Häser, M.; Ahlrichs, R. *J. Comput. Chem.* **1989**, *10*, 104.
(36) Eichkorn, K.; Treutler, O.; Öhm, H.; Häser, M.; Ahlrichs, R. *Chem. Phys. Lett.* **1995**, *240*, 283.
(37) Schäfer, A.; Huber, C.; Ahlrichs, R. *J. Chem. Phys.* **1994**, *100*, 5829.
(38) Kutzelnigg, W.; Fleischer, U.; Schindler, M. *NMR Basic Principles and Progress*; Springer: Berlin, 1990; Vol. *23*, p 165.
(39) Schäfer, A.; Horn, H.; Ahlrichs, R. *J. Chem. Phys.* **1992**, *97*, 2571.
(40) Weigend, F.; Furche, F.; Ahlrichs, R. *J. Chem. Phys.* **2003**, *119*, 12753.
(41) Eichkorn, K.; Weigend, F.; Treutler, O.; Ahlrichs, R. *Theor. Chem. Acc.* **1997**, *97*, 119.
(42) Weigend, F. *Phys. Chem. Chem. Phys.* **2006**, *8*, 1057.
(43) Pople, J. A.; Head-Gordon, M.; Fox, D. J.; Raghavachari, K.; Curtiss, L. A. *J. Chem. Phys.* **1989**, *90*, 5622.
(44) Curtiss, L. A.; Jones, C.; Trucks, G. W.; Raghavachari, K.; Pople, J. A. *J. Chem. Phys.* **1990**, *93*, 2537.
(45) Eriksson, L. A.; Malkina, O. L.; Malkin, V. G.; Salahub, D. R. *J. Chem. Phys.* **1965**, *100*, 5066.
(46) Malkin, V. G.; Malkina, O. L.; Reviakine, R.; Arbuznikov, A. V.; Kaupp, M.; Schimmelpfennig, B.; Malkin, I.; Repiský, M.; Komorovský, S.; Hrobarik, P.; Malkin, E.; Helgaker, T.; Ruud, K. *ReSpect*, version 1.2; Slovak Academy of Sciences: Bratislava, Slovakia, 2010.
(47) Slater, J. C. *Phys. Rev.* **1951**, *81*, 385.
(48) Dirac, P. A. M. *Proc. R. Soc. London, Ser. A* **1929**, *123*, 714.
(49) Vosko, S. H.; Wilk, L.; Nusair, M. *Can. J. Phys.* **1980**, *58*, 1200.
(50) Bahmann, H.; Rodenberg, A.; Arbuznikov, A. V.; Kaupp, M. *J. Chem. Phys.* **2007**, *126*, 011103.
(51) Kossmann, S.; Neese, F. *Chem. Phys. Lett.* **2009**, *481*, 240.
(52) Lambrecht, D. S.; Ochsenfeld, C. *J. Chem. Phys.* **2005**, *123*, 149901.
(53) Izsák, R.; Neese, F.; Klopper, W. *J. Chem. Phys.* **2013**, *139*, 094111.
(54) Guidon, M.; Hutter, J.; VandeVondele, J. *J. Chem. Theory Comput.* **2010**, *6*, 2348.

DOI: 10.1021/ct501137x
J. Chem. Theory Comput. 2015, 11, 1540−1548